The Journal of Supercritical Fluids 133 (2018) 330–342

Contents lists available at ScienceDirect

The Journal of Supercritical Fluids

journal homepage: www.elsevier.com/locate/supflu

Computational fluid dynamic model for glycerol gasification in supercritical water in a tee junction shaped cylindrical reactor

Riza Yukananto*, Artur K. Pozarlik, Gerrit Brem

Thermal Engineering Group, Faculty of Engineering Technology, University of Twente, P.O. Box 217, 7500AE Enschede, The Netherlands

GRAPHICAL ABSTRACT

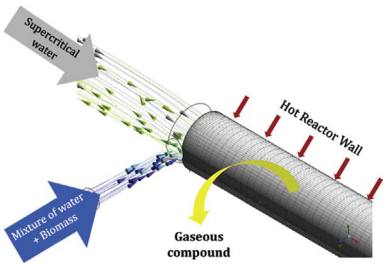

ARTICLE INFO

Keywords:
Supercritical water gasification
Computational fluid dynamic
Glycerol
Cylindrical tee reactor
Sensitivity analysis

ABSTRACT

Gasification in supercritical water is a very promising technology to process wet biomass into a valuable gas. Providing insight of the process behavior is therefore very important. In this research a computational fluid dynamic model is developed to investigate glycerol gasification in supercritical water, which takes place in a cylindrical reactor with a tee junction. The performance of the developed model is validated against experiment, and it shows that the model is able to describe the process very well. The experimental validation shows that the model slightly overestimates the outlet temperature on average by 6% and underestimates the carbon gasification efficiency on average by 16%. The flow behavior in the supercritical water gasification process is successfully described and a sensitivity analysis is conducted. It is revealed that the flow pattern of the process is heavily influenced by gravitational forces which significantly influences mixing and heat transfer.

1. Introduction

Biomass is a renewable energy resource that is expected to play an important role in the global energy mix toward the phasing out of fossil fuels [1–3]. Wet biomass is an attractive, abundant and cheap type of biomass, however, it is a challenge to process it in an energy-efficient way referring to drying as required pretreatment step. Supercritical Water Gasification (SCWG) is a new technology known to have a high potential to convert wet biomass in an efficient manner [4–7]. However, this technology still faces some challenges such as plugging, corrosion and other material issues before it can be utilized in industrial application [6–8]. Several studies indicate that char formation during the (slow) heating up of the biomass may be an important cause of plugging in the process [8–10]. Therefore, it is of major importance to be able to provide insight into flow and reaction behavior during SCWG of biomass with a numerical model.

Several numerical investigations of pure Supercritical Water (SCW) flow in a vertical, horizontal and an inclined pipe are done recently [11–16]. Earlier work of Cheng et al. [11] investigates the influence of mesh structures on the heat transfer in a turbulent SCW flow. It is

Abbreviations: SCWG, supercritical water gasification; SCW, supercritical water; CGE, carbon gasification efficiency; CFD, computational fluid dynamics; TLSM, Tracer Liu-Silva-Macedo; UDF, user defined function

* Corresponding author.
E-mail address: r.yukananto@gmail.com (R. Yukananto).

http://dx.doi.org/10.1016/j.supflu.2017.11.001
Received 21 June 2017; Received in revised form 3 November 2017; Accepted 4 November 2017
Available online 06 November 2017

Nomenclature

A	Pre-exponential factor [1/s]
C_f	Mass flow of carbon in the biomass feed [kg/s]
CGE	Carbon gasification efficiency [%]
D, D_h	Diameter and hydraulic diameter [m]
Ea	Activation energy [kJ/mol]
Fr	Froude number (Dimensionless)
F_2	Blending function [–]
g	Gravity [m/s^2]
Gr	Grashof number (Dimensionless)
Gk, Y_k	Generation and dissipation of k [m^2/s^2]
$G\omega$, Y_ω	Generation and dissipation of ω [1/s]
h	Specific enthalpy [J/kg]
J_i	Diffusion flux [kg/m^2 s]
J_q	Heat flux density [J/m^2 s]
k	Turbulence kinetic energy [m^2/s^2]
k_r	Rate constant of the reaction [1/s]
M	Molar mass [kg/kmol]
p	Pressure [Pa]
q_r	Heat generation or consumption [J/m^3 s]
R	Universal gas constant [kJ/mol K]
S	Strain rate magnitude [–]
S_k, S_ω	User-defined source term of k and ω [–]
t	Time [s]
T	Temperature [K]
u	Velocity [m/s]
v	Kinematic viscosity [m^2/s]
x	Cartesian coordinate [m]

Greek symbols

α^*, α_1	Damping coefficient [–]
β	Temperature exponent (Dimensionless)
β_b	Thermal expansion of the bulk fluid [1/K]
δ_{ij}	Kronecker delta [–]
μ	Dynamic viscosity [Pa s]
μ_t	Eddy viscosity [Pa s]
ρ	Density [kg/m^3]
τ_{ij}	Viscous stress tensor [–]
ψ	Molar rate formation [kmol/m^3 s]
ω	Specific dissipation rate [1/s]

Subscripts

b	Bulk
e	End
s	Start
w	Wall

observed that the performance of the ω-turbulence model strongly depends on the first dimensionless wall distance to the first mesh (y+). In a study of an upward SCW flow in a vertical pipe, Palko and Anglart [12] states that buoyancy plays a small effect in a high mass flow rate. Whereas Wen and Gu [13] find that significant density variation near the pseudo-critical temperature region causes a deformation of the velocity profile and a weakening of turbulence production. This results in a weakening of heat transfer, which is termed a Heat Transfer Deterioration, in their investigation of an upward and downward SCW flow in a vertical pipe. In relation to this study, Zhang et al. [14] study a supercritical fluid flow in a vertical and horizontal pipe, and concludes that an anisotropic model is recommended to model the flow of a supercritical fluid. In parallel like investigations, Jaromin and Anglart [15] observes that heat transfer deterioration can be caused by either the thickening of the viscous sublayer or the influence of buoyancy, and this depends on the fluid flow rate. These results are also summarized in the review article of Huang et al. [16].

Supercritical fluid flow in combination with another compound is investigated by various authors [17–22]. Raghavan and Ahmed [17] investigates a mixing process of n-decane and SCW in a cylindrical tee mixer in a laminar flow. The mixer is comprised of main tube for the SCW and an injection tube for the cold n-decane. Peng-Robinson Equation of State (EoS), Chung's formula, and Silva's formula are used to approximate the fluid density, thermal conductivity and viscosity, and the diffusivity of the compound. They observe that the mixing of different fluids with less than a 100 K temperature difference will not impact the flow field, but a larger temperature difference might. In addition to this study, Moussiere et al. [18] study the influence for both the Arrhenius law and the Eddy Dissipation concept in describing the kinetics for oxidation of dodecane in SCW. They observe that both the Arrhenius law and the Eddy Dissipation Concept are able to give a good prediction in comparison to experimental data. Moreover, Goodwin and Rorrer [19] look into the gasification of xylose in a laminar flow using a generic binary diffusion coefficient and constant thermal properties of water. They observe similar gas compositions, with the exception of CH_4, compared to their experimental study. Another investigation by Yoshida and Matsumura [20] then assess carbon particles deposition in a vertical reactor for oxidation in SCW. They observe the case that particles with the size of 1–10 μm are entrained in a SCW flow. Xiaohui et al. [21] examine the SCWG of glucose in a fluidized bed reactor assuming a uniform wall temperature and 3 competing kinetics. They are able to obtain a similar Carbon Gasification Efficiency (CGE) and gas yield trend compared to their experimental results, though the absolute values are much higher. Recently, Hui et al. [22] implement 7 competing kinetics and investigate the influence of several turbulence models as well as the shape of the injector for glycerol SCWG in a cylindrical tee mixer. They conclude that mixing of the glycerol with the SCW flow prompts the side reaction in a region with low temperature, and that different injector angle can reduce this effect.

Currently, there is limited literature published on numerical methods that addresses the gasification of biomass in SCW. In addition to that, there are no numerical studies that have been performed with the use of a simple global reaction kinetic. A global reaction kinetics is readily available, see [23–27] for more information, and can be utilized in Computational Fluid Dynamics (CFD). On the contrary, detailed reaction kinetics for SCWG is more difficult to obtain.

In this research, a CFD model is developed to investigate the flow pattern, mixing and heat transfer during SCWG of biomass. The gasification takes place in a cylindrical tee mixer with a main line for SCW and an injection line to provide fast heating to the biomass. Furthermore, the proposed CFD model uses glycerol as a simple model compound of biomass and it implements a global reaction kinetics.

The following section presents the methodologies to approximate the fluid properties, the implemented reaction kinetics, the detailed geometry and operating condition of the model. Subsequently, the performance of the model is assessed, the influence of global reaction kinetics to the carbon conversion is analyzed and the process flow behavior is looked into. Finally, the use of an expanded Arrhenius model [28], the influence of gravity and flow velocity in the injector are also studied with a sensitivity analysis.

2. Modelling approach

A chemically reacting turbulent flow can be modelled and solved at each point in space and time by specifying its pressure, mass, temperature, velocity, and species concentration. The commercial CFD

code ANSYS Fluent 16.0 is used to simulate the gasification of glycerol in supercritical water. The following section briefly presents the mathematical description of equations that govern this system and the relevant turbulence models. Selection of fluid properties, reaction kinetics, and discretization scheme are also presented here.

2.1. Governing equations

The simplest form of mass, species, momentum and energy conservation equations are given in the following equations [29]. The mass conservation is described as the product of local flow velocity and density without considering gravity. Species conservation takes into account that formation and consumption of species take places during chemical reactions. The momentum conservation equation contains the convective momentum transfer, its pressure tensor and the effect of gravity. Together with the mass conservation equation, it leads to the often used Navier-Stokes equation. The energy conservation considers the conductive and convective energy transfer, energy change due to pressure, viscous dissipation and chemical reactions. These equations are shown in Eqs. (1)–(4) respectively.

$$\frac{\partial \rho}{\partial t} + \nabla(\rho \vec{u}) = 0 \tag{1}$$

$$\frac{\partial \rho_i}{\partial t} + \nabla(\rho_i \vec{u}) + \nabla \vec{j_i} = M_i \omega_i \tag{2}$$

$$\frac{\partial (\rho \vec{u})}{\partial t} + \nabla(\rho \vec{u} \otimes \vec{u}) + \nabla \bar{\bar{p}} = \rho \vec{g} \tag{3}$$

$$\frac{\partial (\rho h)}{\partial t} - \frac{\partial p}{\partial t} + \nabla(\rho \vec{u} h + \vec{j_q}) + \bar{\bar{p}} : \nabla \vec{u} = q_r \tag{4}$$

$$\bar{\bar{p}} = p\,\delta_{ij} + \tau_{ij} \tag{5}$$

2.2. Turbulence modelling

Continuous fluctuation of velocity is a defining feature in a turbulent flow and this leads to a fluctuation of other flow properties. The Reynold-Averaged Navier-Stokes (RANS) method splits the flow properties of the Navier-Stokes equations and subsequently implements the Favre averaging, and finally implements a model that can describe its *Reynold stresses* term [29].

Literature shows that to model a flow of a supercritical fluid, it is recommended to use either the Shear Stress Transport (SST) k-ω model or the Reynold Stress Model [12–14,30,31]. In relation to this, Zhang et al. [14] state that the Reynold Stress Model provides less error when predicting heat transfer in comparison to RNG k-ε model. On the other hand, Wang et al. [31] reports that the SST k-ω model gives an improved heat transfer prediction for supercritical fluid in comparison to the RNG k-ε model. In addition, Jaromin and Anglart [15] show that the k-ω SST model give a very accurate heat transfer and flow prediction in an upward flow in a cylinder whereas Wen et al. [13] proves that this model also performs well in a downward flow in a cylinder. Furthermore, Dutta et al. [30] observes that the SST k-ω in some cases outperforms the RSM model. The SST k-ω is therefore selected for this research. SST k-ω is a two equations RANS model that uses the turbulent kinetic energy and specific dissipation and defines its turbulence viscosity to solve the RANS equations [Eqs. (6)–(8)] [28].

$$\frac{\partial (\rho k)}{\partial t} + \frac{\partial (\rho k u_i)}{\partial x_i} = \frac{\partial}{\partial x_j}\left(\Gamma_k \frac{\partial k}{\partial x_j}\right) + G_k - Y_k + S_k \tag{6}$$

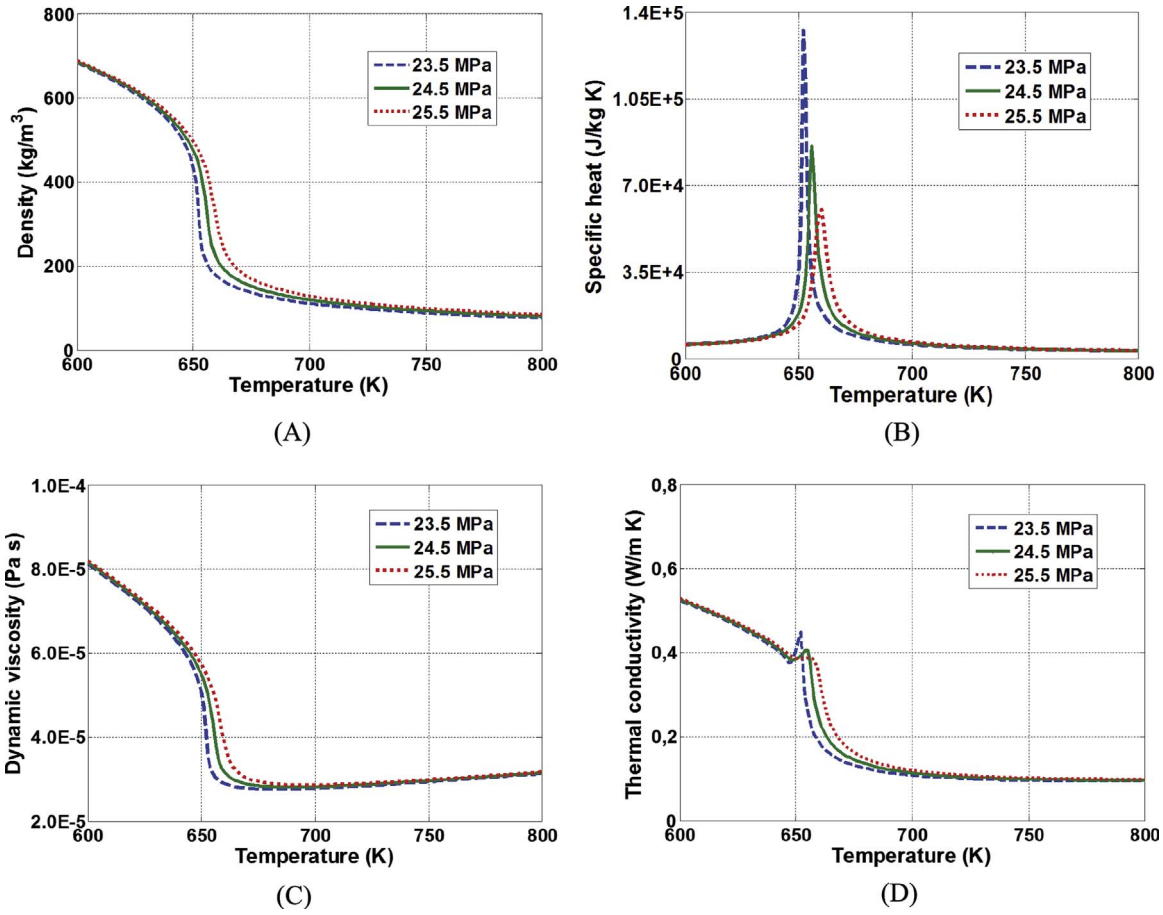

Fig. 1. Properties of water during the transition from subcritical to supercritical condition.

$$\frac{\partial(\rho\omega)}{\partial t} + \frac{\partial(\rho\omega u_i)}{\partial x_i} = \frac{\partial}{\partial x_j}\left(\Gamma_\omega \frac{\partial \omega}{\partial x_j}\right) + G_\omega - Y_\omega + S_\omega \tag{7}$$

$$\mu_t = \frac{\rho k}{\omega} \frac{1}{\max\left[\frac{1}{\alpha^*}, \frac{SF_2}{\alpha_1 \omega}\right]} \tag{8}$$

A flow of supercritical fluid usually involves a high heat transfer from the wall and a large property variation of the fluid near the wall. Therefore, one of the most important aspects when solving the supercritical fluid flow is to resolve the flow near the boundary properly. In the case of implementing the SST k-ω model, strong influences of the first mesh size on the overall heat transfer were observed [11,12]. Palko and Anglart [12] states that the y^+ value has to be lower than 1.

2.3. Fluid properties

The thermodynamic and transport properties of water are changing significantly during its transformation to supercritical condition. The viscosity and density largely decrease at this condition, which leads to an improvement in mass transfer [32,33]. The thermal conductivity is reduced and a large variation of its specific heat capacity can be noticed [6,7]. Fig. 1 visualizes these behaviors for different operating pressures and temperatures.

IAPWS-IF97 is recommended and is used for the calculation of the density, specific heat capacity and enthalpy of water [34]. This method divides the properties of water into 5 separate regions and calculates its properties based on different sets of equations respectively for each region [35]. The viscosity of water is calculated using the IAPWS 1985 formulation revised in 2003 and its thermal conductivity is calculated with the IAPWS 1985 formulation revised in 1998 [35].

Several authors recommended to approximate the properties of the other compounds with the Peng-Robinson EoS [17,36]. The values of thermal conductivity and viscosity of other compounds are approximated using method proposed by Chung et al., see [37] for further information. The real gas specific heat capacity and enthalpy are calculated using the method proposed by Aungier, see [38,39] for further information. The coefficients used to calculate the specific heat capacity and enthalpy at STP are obtained from the NASA thermodynamic database, see [40] for furhter information.

In high temperature range, the SCW is able to dissolve organic compounds [1,41]. The diffusion coefficient of an organic compound in water at normal conditions is enchanced by a factor of 100 when the water is in its supercritical condition. There are two methods available to approximate the temperature-dependant diffusivity of compound in SCW, the He's method and the Tracer Liu-Silva-Macedo (TLSM) method, see [42,43]. Since the He's method does not provide an accurate prediction at the lower temperature range, thus, the TLSM method is chosen, and further information can be found in [43].

All the above mentioned properties are calculated at a constant pressure and incorporated as tabulated data into a User Defined Function (UDF). It is assumed that the change of the properties are negligible because the flow velocity is relatively slow and the pressure losses due to friction are minor.

2.4. Reaction kinetics

Due to the excess of water, it is assumed that the gasification reaction proceeds with a pseudo first-order kinetic behavior, see [8,23] for further information. Experimental investigations show that no char is produced during SCWG of glycerol [25,26]. Simao et al. [27] shows that the pre-exponential factor (A) and the activation energy (Ea) for the kinetics of glycerol gasification are $10^{5.9 \pm 1.3}\,s^{-1}$ and 104.5 ± 20.3 kJ/mol respectively. During the experiment, a plug flow condition was assumed and the research was conducted applying isothermal condition, which implies that it is a kinetically-limited reaction rate. The empirical reaction stoichiometry was derived from the experimental results done by Simao et al. [27]. Calculation formulas for the kinetics and reaction stoichiometry are shown in Eqs. (9) and (10) respectively.

$$k_r = A \quad exp^{-\frac{Ea}{RT}} \tag{9}$$

$$C_3H_8O_3 + 1.0781\,H_2O \rightarrow 4.441\,H_2 + 0.3186\,CH_4 + 1.2619\,CO + 1.4196\,CO_2 \tag{10}$$

2.5. Experimental data, geometry and boundary

This investigation is done to simulate gasification of glycerol in supercritical water as was experimentally investigated by Simao et al. [27]. The experimental investigation is done in a reactor that has a shape of a cylindrical tee mixer. This consists of a main cylindrical tube with an inner diameter of 10.85 mm and a small injection tube with an inner diameter of 4 mm. The main tube delivers supercritical water that provide a fast heat-up to the biomass feed that comes from the injection tube. The main tube is positioned horizontally and the injection tube enters it perpendicular to the flow. The injection tube is located at a

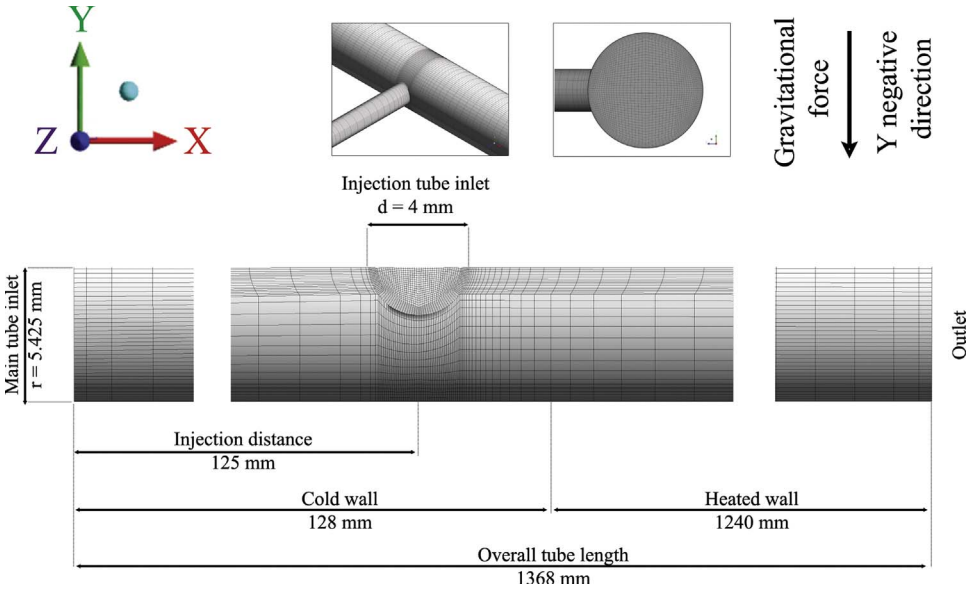

Fig. 2. Half domain schematic of the reactor.

distance of 0.125 m from the inlet of the main tube. The overall length of the tube is 1.368 m and only the 1.24 m of tube wall after the injection point is heated. The schematic of the reactor is visualized in Fig. 2.

The experiments are performed at a flow rate of 4 kg/h with an inlet temperature of 699 K in the main tube and a flowrate of 1 kg/h with an inlet temperature of 288 K in the injection tube. The injection tube delivers a flow containing 50 wt-% glycerol that corresponds to a total of 10 wt-% glycerol in the overall system. The experiments are done at a pressure of 25 MPa.

2.6. Numerical method

Volumetric reaction with a laminar-finite rate is used for the turbulence chemistry interaction. Input for both the reaction and the stoichiometry are stated in Section 2.4. For the calculation, the "Coupled" pressure and velocity coupling method is used. The conservation equations are discretized and are solved with second order upwind scheme interpolation. The residual criteria for convergences are set to be 10^{-4} for the continuity and 10^{-6} for the rest of the equations. The BCG stabilization method is used for all equations.

2.7. Data analysis

Both outlet temperature and CGE are used to validate the model. CGE represents the ratio of the total converted carbon at the end of the process to the fed carbon. This definition is shown in Eq. (11).

$$CGE = 1 - \frac{C_{f,e}}{C_{f,s}} \tag{11}$$

The natural convection plays an important role in a supercritical flow with low mass flux, see [12,44,45] for further information. The Grashof number can be applied to quantify the influence of buoyancy to the flow field. The Grashof number approximates the ratio of buoyancy force that might happen because of the temperature gradient to the viscous force, and is shown in Eq. (12). This dimensionless parameter is commonly used in conjunction with the Reynolds number [45]. A ratio of Grashof to Reynolds number that is higher than unity represents a significant influence of the flow field due to buoyancy.

$$Gr = \frac{g\,\beta_b\,D^3(\nabla T)}{\nu_b^2} = \frac{(\rho_w - \rho_b)\overline{\rho_b}\,g\,D_h^3}{\overline{\mu_b}^2} \tag{12}$$

Density variations due to the major temperature difference that takes place near the pseudo-critical point can lead to a non-unity density ratio. This can modify the flow field as eddies in the flow move toward the denser fluid and hence, the entrainment pattern is changed favoring the denser fluid [46,47]. Depending on the flow condition, this flow entrainment pattern can be transmitted upstream of the flow and significantly affect the flow characteristic. The Froude number can be used here to identify the type of flow and it is defined in Eq. (13). A Froude number below unity represents a slow or tranquil flow and any disturbances in the flow will be transmitted upstream.

$$Fr = \frac{u}{\sqrt{gD}} \tag{13}$$

3. Results and discussion

This section presents the flow behavior inside the reactor during the gasification. To begin with, the mesh independency is checked. Then the performance of the model is assessed based on a comparison between the predicted temperature and the CGE level against the experimental data from Simao et al. [27]. Finally, a sensitivity analysis of the model is presented.

3.1. Mesh independency

A mesh independency study is done in order to verify that the

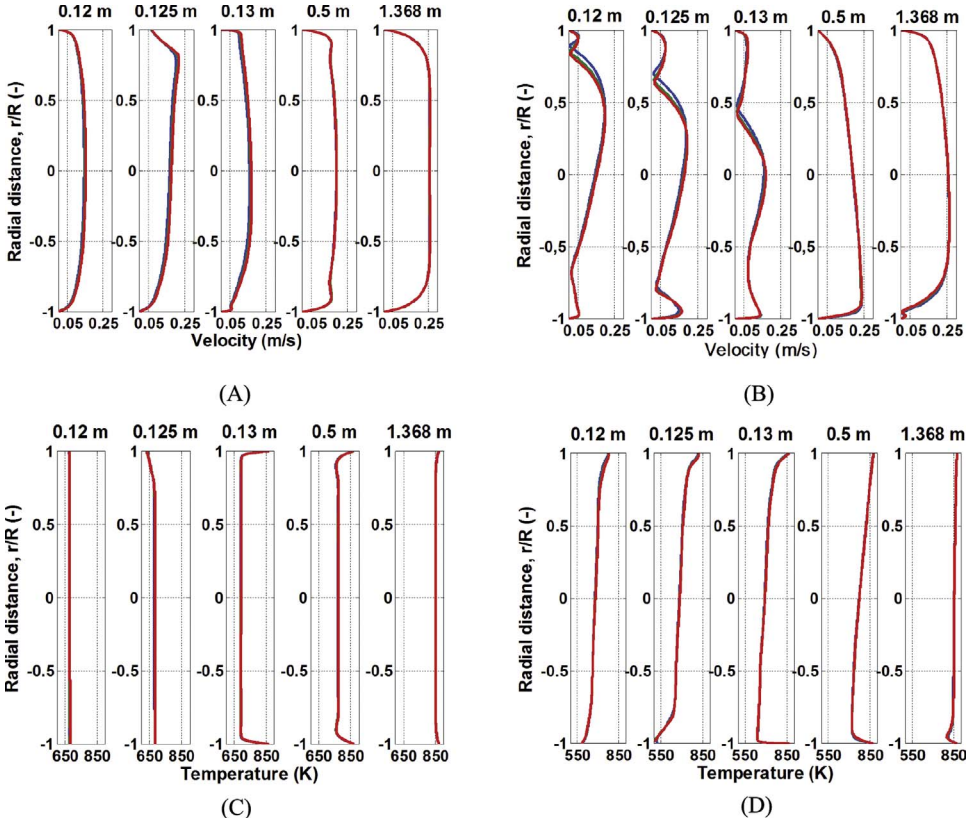

Fig. 3. (A–D) Flow field profile at axial coordinate of 0.12 m, 0.125 m, 0.13 m, 0.5 m, 1.368 m. (▬) Mesh 1: 2.86 M elements; (▬) Mesh 2: 6.49 M elements (▬) Mesh 3: 13.3 M elements. (A-B) Horizontal and vertical velocity profile. (C-D) Horizontal and vertical temperature profile.

chosen mesh provides adequate spatial resolution and it does not influence the result. Each mesh is refined by doubling the number of the elements in the radial direction. The three meshes comprise of: 1) 2.9 million elements; 2) 6.5 million elements; 3) 13.3 million elements. The mesh independency study is done for non-reacting flow, since preliminary investigation showed that the velocity and temperature flow fields do not vary considerably for a flow with and without reactions.

The inlet flow rate of the SCW is equal to 4 kg/h and it enters the reactor at a pressure of 25 MPa and a temperature of 699 K. The mixture of water and glycerol is injected with a temperature of 288 K and a mass flow rate equal to 1 kg/h. Fig. 2 shows the geometrical dimensions, injection location and coordinate system. Fig. 3 presents the velocity and temperature distributions in the vertical and horizontal direction inside the tube.

The velocity profile in the horizontal direction shown in Fig. 3A does not seem to change significantly with different mesh sizes. A peak velocity profile near the injection can be observed in this figure. This peak takes place due to a movement of the SCW fluid from the main tube into the injection tube. The velocity profile in the vertical direction shown in Fig. 3B indicates that by decreasing element sizes there is a minor velocity change near the injection point. This, however, does not result in a significant temperature change as visualized in Fig. 3C & D. The maximum difference in temperature obtained from these three different meshes amounted to does not exceed 10 K.

The vertical velocity profiles for positions of 0.12 m up to 0.13 m show that the peak velocity in the bulk flow is moving downward along the axial direction. This takes place due to the density difference between the SCW fluid and the injected fluid. The colder (denser) injected fluid goes to the bottom of the tube and creates a swirling motion upstream of the injection location. This swirling motion pushes the incoming SCW to flow to the top of the tube. Subsequently, at the injection point, SCW that flow on the top of the tube will move downward to fill the void left by the swirling injected fluid.

Visualization of these phenomena is also shown in Fig. 4 that presents the streamline coming from the main inlet (grey line) and injection inlet (colored line). The minor differences between the investigated meshes for velocity and temperature profiles suggest that the result are mesh independent and the mesh with the biggest element size provides sufficient spatial resolution and therefore can be used for final research.

3.2. Model validation

The study is done for several different outer reactor wall temperatures, namely: 773 K, 823 K, 873 K, 923 K and 963 K, and in combination with the operating conditions that are mentioned in Section 3.1. Experimental values used for the validation are obtained from the work of Simao et al. [27] and Hui et al. [22]. Fig. 5A shows a comparison of numerical and experimental outlet temperature for various wall temperatures. It can be seen that the simulations slightly overestimate the outlet temperature by approximately 6%. This can be due to two things: a) heat transfer deterioration causes the non-uniformity of the experimentally investigated inner reactor wall temperature whereas the developed model imposes a uniform wall temperature [15]; b) wall thickness of the tube, which is not considered in the model, might play an important role to reduce the overall heat transfer. It should also be noted that the numerical results may in fact be in agreement with the experimental data as the measurement error in [22,27] was not given.

The discrepancies of the CGE between numerical and experimental range from 3% to 16% as is visualized in Fig. 5B, except at reactor wall temperature of 773 K where about than 50% can be observed. The main reason for such behavior is the reaction kinetics that is described in Section 2.4. It provides a significant difference in reaction speed at temperatures lower than 780 K. Since the model predicted higher temperature for this condition than the experiment (by ± 30 K), consequently the CGE is also enhanced. Therefore, it is important to perform a CGE comparison based on the outlet temperature. This will be discussed in Section 3.3.1.

A comparison of gas yield obtained from numerical and experimental results are presented in Fig. 5C. Neglecting a minor difference for H_2 yield, the overall predicted values are very similar. It can be concluded that a model that assumes a single phase flow in combination with the SST k-ω turbulence model is able to provide an accurate behavior of glycerol gasification in SCW. Moreover, it is revealed that the implementation of a global kinetics with simple reaction stoichiometry is able to provide a similar result to the values obtained from experimental investigation.

It was mentioned in Section 3.1 that the SCW flow may experience a swirling motion near the injection point. Fig. 6A shows the axial direction velocity streamline of a flow with a reactor wall temperature of 873 K. It can be seen that the some part of the injected glycerol/water mixture experiences a negative velocity, which means that this flow moves upstream toward the inlet of the main tube. Fig. 6B presents the temperature streamline from the top view of the reactor. It can be noted that there is a flow separation after the injection. This is further confirmed in Fig. 6C where the temperature streamline from the front view of the reactor is depicted. Another flow separation that creates a left and right swirling motion as the injected fluid flows along the axial direction is presented there.

Fig. 7A presents a front view of the velocity vector colored with temperature field at the injection point. This figure suggests that the first swirling motion arises as the injected fluid, that has high density and is slower, moves to the bottom of the tube due to gravity. Fig. 7C shows that the Froude number near the injection is below 1, which means that this is a tranquil (unforced) flow. This means that the fluid movement in the axial direction is so slow that it cannot suppress the swirling motion. Because of that, the swirl pattern is moved upstream

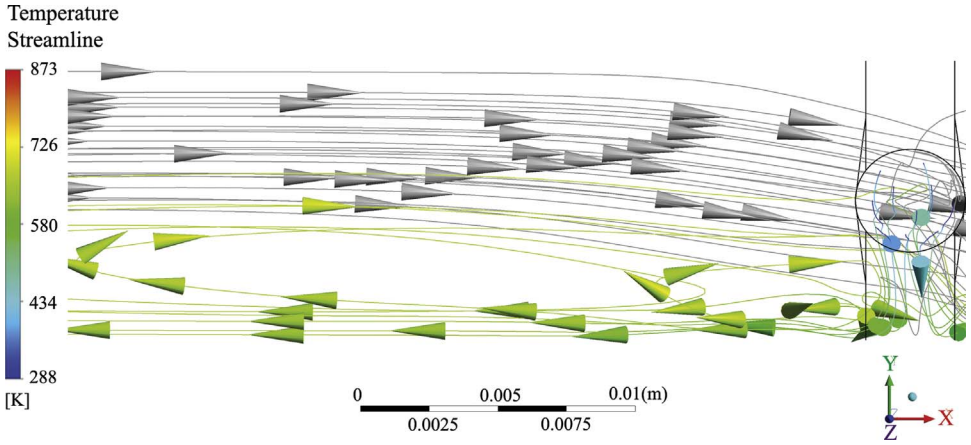

Fig. 4. Streamline for non-reacting flow with reactor wall temperature of 873 K. (▬) Streamline of SCW; (▬) Streamline of injected glycerol and water.

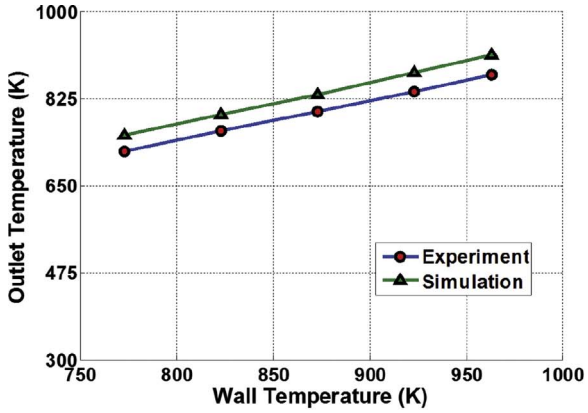

(A)

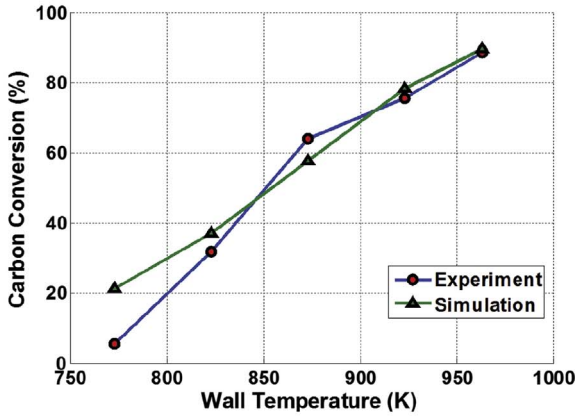

(B)

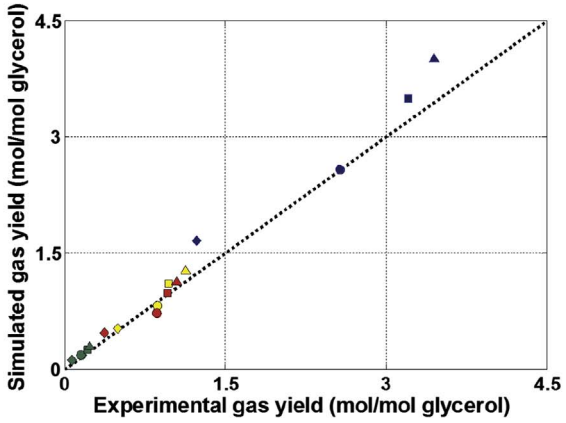

(C)

Fig. 5. (A-C) Comparison of results obtained from numerical and experimental [27] result with SCW flow at 699 K with 4 kg/h and 50 wt-% injected glycerol at 288 K with 1 kg/h at 25 MPa. (A) Wall temperature vs outlet temperature. (B) Wall temperature vs CGE. (C) Gas yield at: ◆ 823 K, ●873 K, ■923 K, ▲963 K. (—) H2, (—) CO_2 (—) CO (—) CH_4.

and creates even bigger swirls (eddies) near the inlet of the main tube. This swirling motion of the fluid is illustrated in Fig. 7D. Furthermore, the swirling motion acts together with the gravitational force to drag the incoming SCW down. This generates the diagonal fluid movement shown in Fig. 7A.

Subsequently, the fluid at the top of the tube at downstream location, which has been heated up by the hot reactor wall, is forced to swirl backward. This results in a minor temperature increase near the top of the tube. This concept is supported by the result presented in Fig. 8A and B. These illustrate the ratio of Grashof and Reynolds number, which are a measure of the buoyancy influence on the flow pattern, along the horizontal and vertical direction respectively. Value above one that indicates an intense buoyancy effect, can be observed on the injection location at an axial distance of 0.125 m in Fig. 8A. The sharp drop near a radial distance of −1 is due to the fact that temperature (density) is almost constant there while the velocity is increasing significantly. Fig. 8B also shows that the influence of buoyancy is significant for both the bottom and the top of the pipe near the injection.

The second swirling motion in Fig. 7B, which takes places downstream of the pipe, occurs due to the difference of fluid density near the wall and in the bulk flow. It can be discerned that the fluid near the tube wall has a high temperature, and thus a low density. This fluid moves then quickly upward due to buoyancy effect. After it reaches the top, it is dragged by the incoming flow in the middle of the tube and then slowly moves downward due to the gravity. After it reaches the bottom of the tube, the same cycle is repeated. Also according to Fig. 8A and B at an axial distance of 0.5 m, the Gr/Re^2 above 1 near the tube wall can be noted. Taking this into account, it can be concluded that buoyancy indeed plays an important role in facilitating the swirling motions. It can also be concluded that the overall heat transfer in the tube is significantly improved due to the mixing induced by these swirling motions.

Fig. 9A and B presents the temperature contour of a flow with a reactor wall temperature of 873 K from the top and side view respectively. It can be seen that in the vertical direction, the bulk flow has a higher temperature near the top of the tube and this is gradually reduces as it gets closer to the bottom tube. The reaction rate in the vertical direction shown in Fig. 10B is bound to portray a similar behavior, as reaction rate is highly dependent on temperature. Reaction rate at an axial distance of 0.125 m in Fig. 10B, however, does not show this behavior. The reaction rate temporarily decreases and then increases again as it proceeds toward the bottom tube. This milder reaction in the middle of the tube takes place due to the fact that glycerol does not have sufficient time and has not yet diffuse from the bottom tube to the top region.

In contrast, the temperature distribution of the bulk flow along the reactor as presented in Fig. 9A is uniform, except for the flow near the tube wall. Consequently, the rate of reaction near the wall is almost 5 times bigger than the reaction rate in the bulk flow, as is depicted in Fig. 10A. This figure also shows that the gasification reaction has already started to take place at an axial distance of 0.125 m at location closest to the injection (dimensionless radial distance of −1). This implies that the injected fluid has a sufficiently high temperature to start the reaction at that location. Therefore, it can be concluded that some part of the SCW from the main tube enters the injection tube, and consequently it recirculates at that location and partially heats up the injected flow.

3.3. Sensitivity analysis

Influence of the kinetic description to the obtained result is investigated in this section. In addition to this, the importance of the imposed gravitational force and the injection velocity to the flow behavior is looked into.

3.3.1. Influence of temperature dependent Arrhenius Formula

Section 3.2 showed that there are some inconsistencies in the outlet temperature obtained from simulations and experiments. It is also observed that at a low temperature range, there is a significant CGE difference from the results that are obtained from simulations and experiments. To account for this, a CGE comparison that uses the corresponding outlet temperature is displayed in Fig. 12.

In Addition to this comparison, an extended model that uses an expanded Arrhenius formula is investigated and the results are presented using the corresponding outlet temperature in Fig. 12. This expanded Arrhenius formula is shown in Eq. (14). This formula is used to

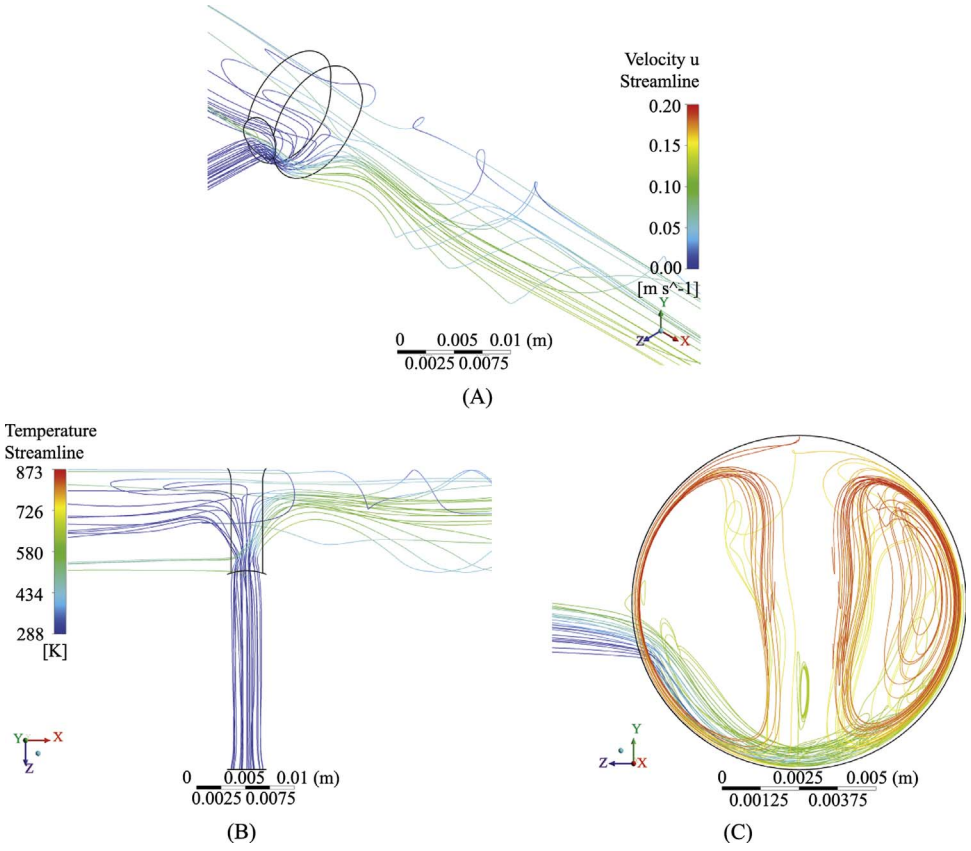

Fig. 6. (A–C) Streamline for flow with reactor wall temperature of 873 K. (A) Velocity streamline and (B-C) temperature streamline.

account and correct for the deviation of predicted and the experimental data as is shown in Fig. 11A. The deviation of kinetics value obtained from the experimental data and the Arrhenius formula is fitted into a 4th order polynomial curve as can be seen in Fig. 11B. The equation used to describe this curve is shown in Eq. (15) and is used as an expansion factor in Eq. (14). This expansion factor is only activated at the temperature of 760–840 K, since here the reaction occurs intensely.

$$k_{r,expanded} = AT^{\beta} exp^{-\frac{Ea}{RT}} \tag{14}$$

$$\beta = 0.03898\,T^4 + 0.0175\,T^3 - 0.1213\,T^2 - 0.02756\quad T + 0.05055 \tag{15}$$

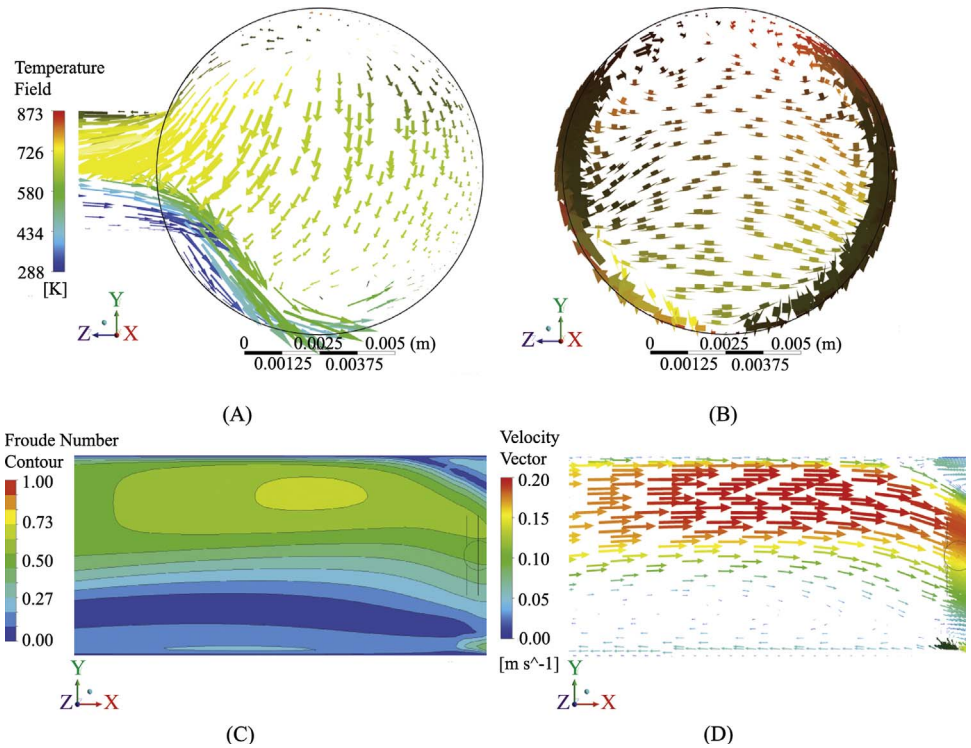

Fig. 7. (A–D) Flow with reactor wall temperature of 873 K. (A-B) Front view of velocity vector colored with temperature variable at 0.125 m and 0.5 m. (C) Contour plot of Froude number near injection. (D) Vector flow field near injection.

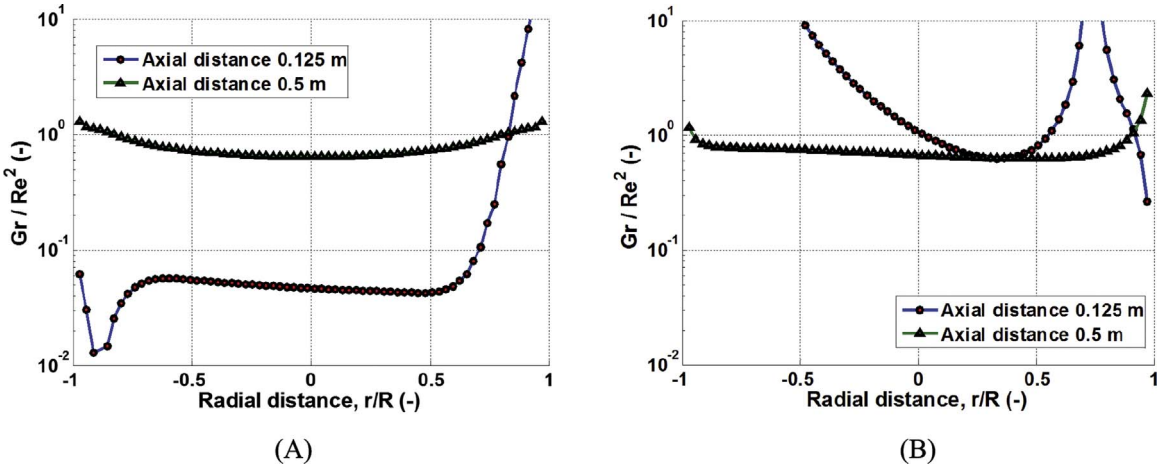

Fig. 8. (A-B) Ratio of Grashof number and Reynolds number for horizontal and vertical radial direction for a flow with reactor wall temperature of 873 K.

As it can be seen from Fig. 5A, wall temperatures of 773 K, 823 K and 873 K corresponds to outlet temperatures of 752 K, 793 K and 834 K respectively. Observing the comparison made in Fig. 12, numerical results with standard Arrhenius formula demonstrates CGE underestimation of about 18%, 34% and 20% respectively, based on the above mentioned outlet temperatures. Moreover, a noticeable difference of CGE at outlet temperature of 793 K is revealed. In contrast to this, utilizing the expanded Arrhenius formula leads to leads to CGE underestimation of only 10%, 23% and 15% for the respective outlet temperature

The average accuracy of the CGE predictions using the standard and expanded Arrhenius formula are 24% and 16% respectively. Implementing the expanded Arrhenius formula is shown to improve the prediction accuracy of approximately 8%. However, Fig. 12 also indicates that only minor improvement follows for the reaction that takes place in higher temperature region.

The discrepancies of the CGE comparison might be due to the fact that the kinetics that is used was obtained through experiment that assumes a uniformly distributed glycerol with an isothermal condition [27]. However, Fig. 6C showed that concentration and temperature field inside the reactor does not follow these assumptions. This non-uniformity might lead to an Arrhenius formula (the pre-exponential factor and activation energy) that predicts lower kinetics value than what is occurring during the experiment. Therefore, a sensitivity analysis related to the pre-exponential factor and activation energy might be useful. Additional reason for these discrepancies might be due to the lack of phase-mass boundary interaction, which can be obtained through a multiphase flow modelling.

3.3.2. *Effect of direction of gravitational force*

Several studies stated that char formation can take place during SCWG of biomass due to polymerization reactions that occur at subcritical conditions and that a fast heat up of wet biomass can reduce this effect [9,10]. It has been discussed in Section 3.2 that gravity promotes the swirling motions which in consequence improves both the heat transfer due to mixing enhancement and the residence time of the injected glycerol. Therefore, several different cases that use different gravitational forces are investigated and are listed in Table 1. The flow behaviors of these cases are presented in Fig. 13A–E respectively.

It can be noticed that simulation based on case A, D and E provides a similar flow pattern. At these conditions, however, the back swirling motion near the injection point is eliminated. Fig. 13H also shows that the outlet temperatures obtained from case A and D are very similar to the reference case. Even though the flow patterns obtained from of simulations based on case A and E are almost identical, the x-direction gravitational force in case A induces a swirling motion from the SCW flow that comes from the inlet of the main tube and case E does not possess this behavior, as are portrayed in Fig. 13F and G respectively. This swirling motion occurs due to faster fluid movement near the tube wall, i.e. along its axial direction and also slightly ahead of the injection location, compared to the bulk flow as. This leads to a significant outlet temperature differences from case A and E.

Simulation that is based on case B generates an extremely intense back swirl motion, because the tranquil flow essentially attempts to go upward against gravity. In contrast to this, simulation based on case C experiences a slight back swirl near the injection point. In addition to this, further down the tube, there will be a similar flow separation reference case and was shown in Fig. 6C. This creates top and bottom swirling motions along the length of the tube. These different flow patterns obtained from case A-D only lead to a minor difference in outlet temperature of up to approximately 5 K as is shown in Fig. 13F. Case E, however, predicted lower temperature of approximately 50 K in comparison to the other cases. Fig. 13I presents the residence time of the injected flow from these five different conditions. These residence

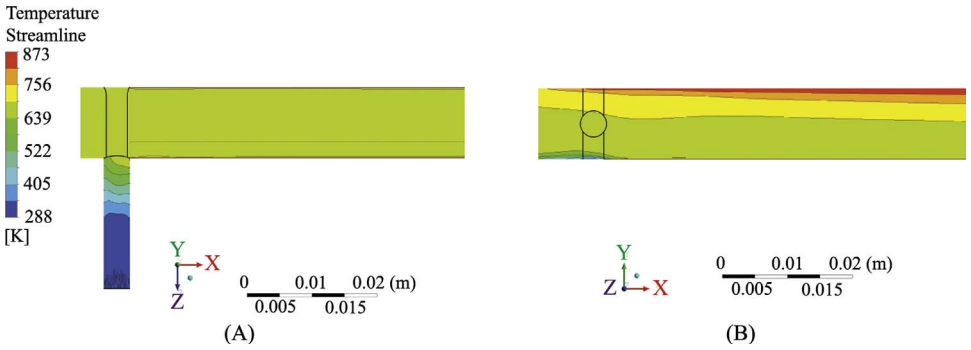

Fig. 9. Temperature contour in a middle XZ plane (A) and XY plane (B).

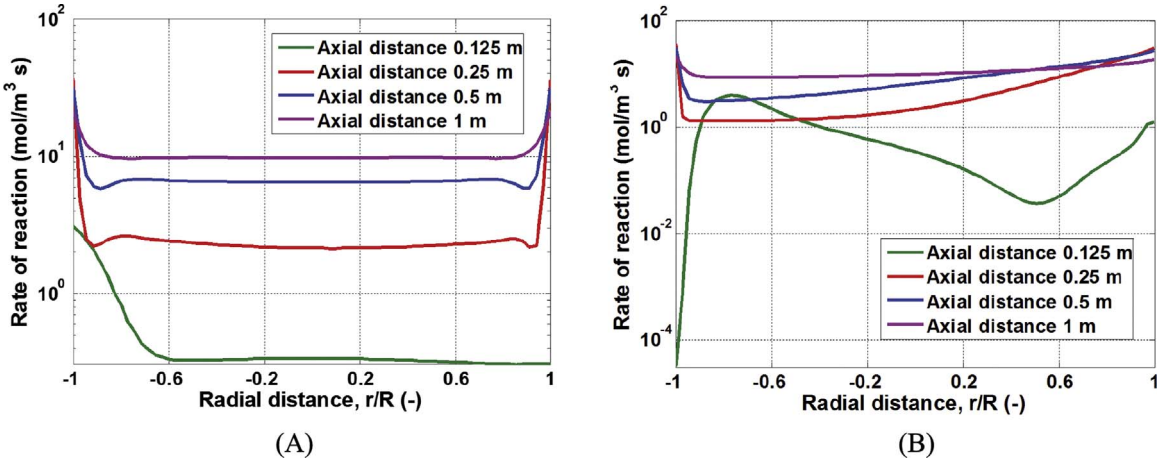

Fig. 10. (A-B) Rate of reaction for horizontal and vertical radial direction for a flow with reactor wall temperature of 873 K.

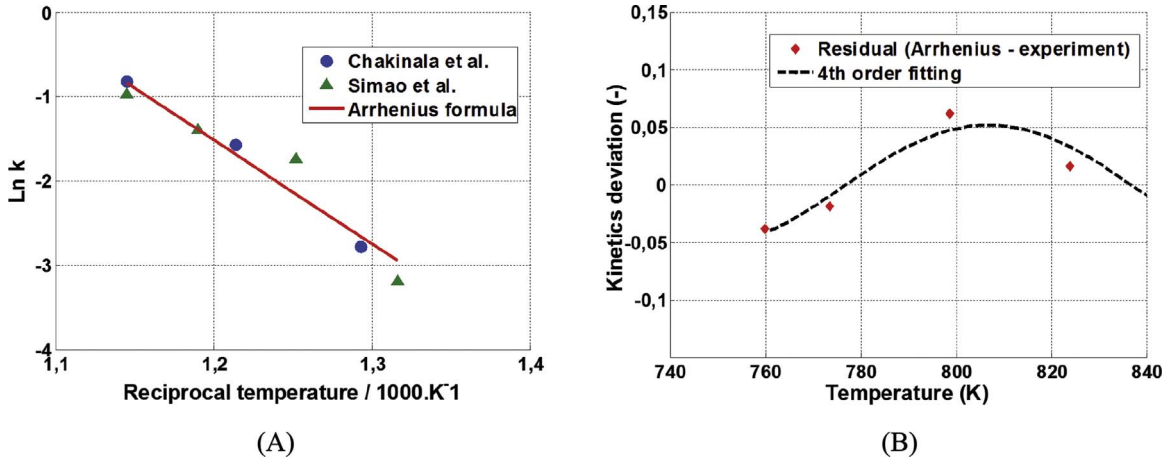

Fig. 11. (A) Kinetics of SCWG of glycerol from Simao et al. [27] and Chakinala et al. [25] (B) Fitted 4th order polynomial for the deviation of kinetic.

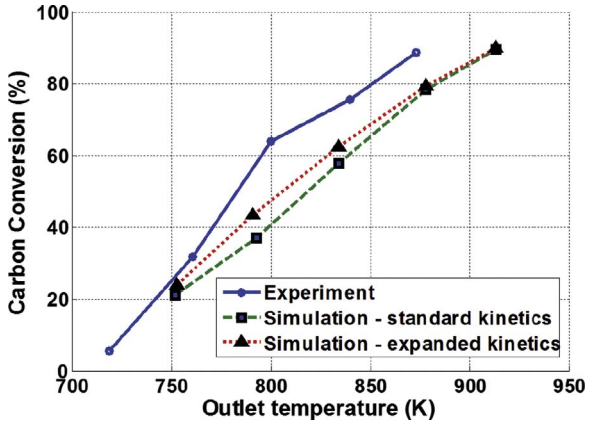

Fig. 12. Comparison of CGE versus outlet temperature for results obtained from numerical and experimental for flow a with a reactor wall temperature of 873 K.

Table 1
List of investigated casesName and properties.

Case	Reference	A	B	C	D	E
Gravitation	y-positive	x-positive	x-negative	z-positive	z-negative	non

times are obtained from the "Time" variable in the streamline provided in ANSYS CFD-Post, discounting streamlines that are stuck in a continuous swirl or flowing with a creeping motion on the tube wall. It can be seen that simulations that use gravitational force in the x-positive and x-negative direction have the shortest and longest residence time, respectively. It has to be noted that the latter also leads to an everlasting continuous swirl for some of its streamlines, and therefore is not recommended. Taking all of this into account, it is advised that the reactor tube is located horizontally with the injection tube entering from either the side or the bottom part of the main tube (y-positive or z-negative gravitational force).

3.3.3. *Effect of glycerol injection speed*

Fig. 6C in Section 3.2 shows that a part of the SCW flow that comes from the inlet of the main tube enters the injection tube and recirculates there. This leads to a gradual partial heating of the injected glycerol. This is a disadvantages when gasifying a biomass compound as slow heating can lead to char formation [10]. This is especially true for flow condition with low mass flux as is commonly done in a laboratory scale investigations. Therefore, two additional geometries, one with a 2.8 mm inner diameter injection tube and the other with a 5.6 mm inner diameter of injection tube, are investigated. The same injection flowrate of 1 kg/h is used for both cases.

The latter is tested due to the fact that a higher injection velocity creates a more forceful flow that will not transmit the disturbance near the injection point upstream to the injection tube. The former is tested due to a premise that lower injection velocity creates a smaller disturbance near the injection point, thus reducing the swirls adjacent to it and consequently reducing the SCW flow that comes into the injection tube. The temperature streamlines for both geometries are visualized in

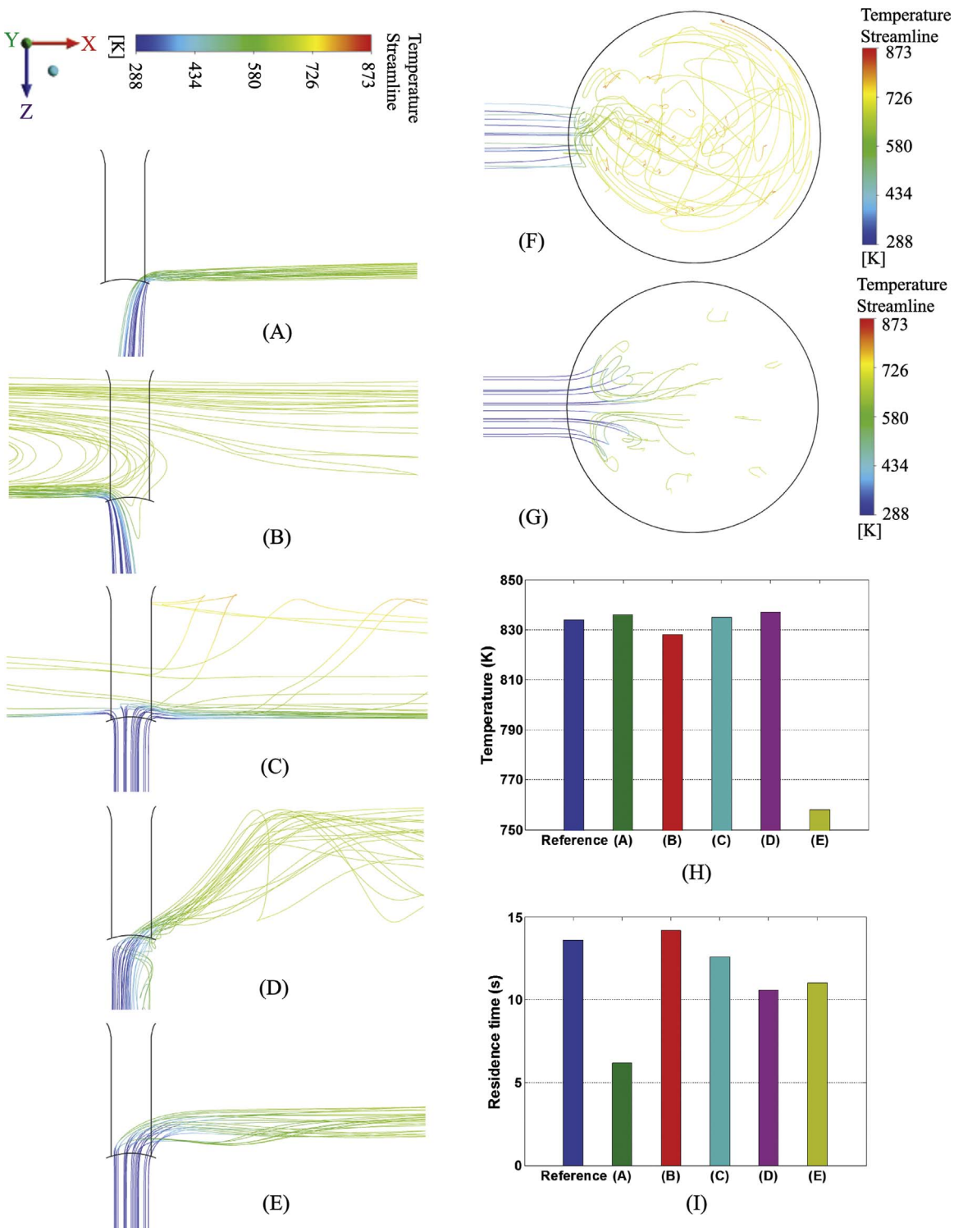

Fig. 13. (A–G) Flow with reactor wall temperature of 873 K. (A–E) Temperature streamlines for case A, B, C, D and E respectively. (F–G) Front view temperature streamline for case A and E respectively. (H–I) Comparison of outlet temperature and residence time from 6 different gravitational forces.

Fig. 14A and B, respectively.

These figures show that the case with a larger injection tube leads to a more intense recirculation inside the injection tube that causes a longer partial heating of the incoming flow. This can be deduced from the high temperature streamlines inside the injection tube. On the other hand, the second case reduces the recirculation inside the injection tube and thus reduces the partial heating. This, however, leads to a decrease in residence time as is shown in Fig. 14D. The changes of the injection geometry provides almost no changes to the outlet temperature, see Fig. 14C. Therefore, it is suggested to reduce the inner diameter of the injection tube or to increase the flowrate of the injection tube, as these options can reduce the partial heating induced by the flow recirculation.

4. Conclusion

The model developed in this research assumes a single phase flow with a global kinetics mechanism. Several different operating

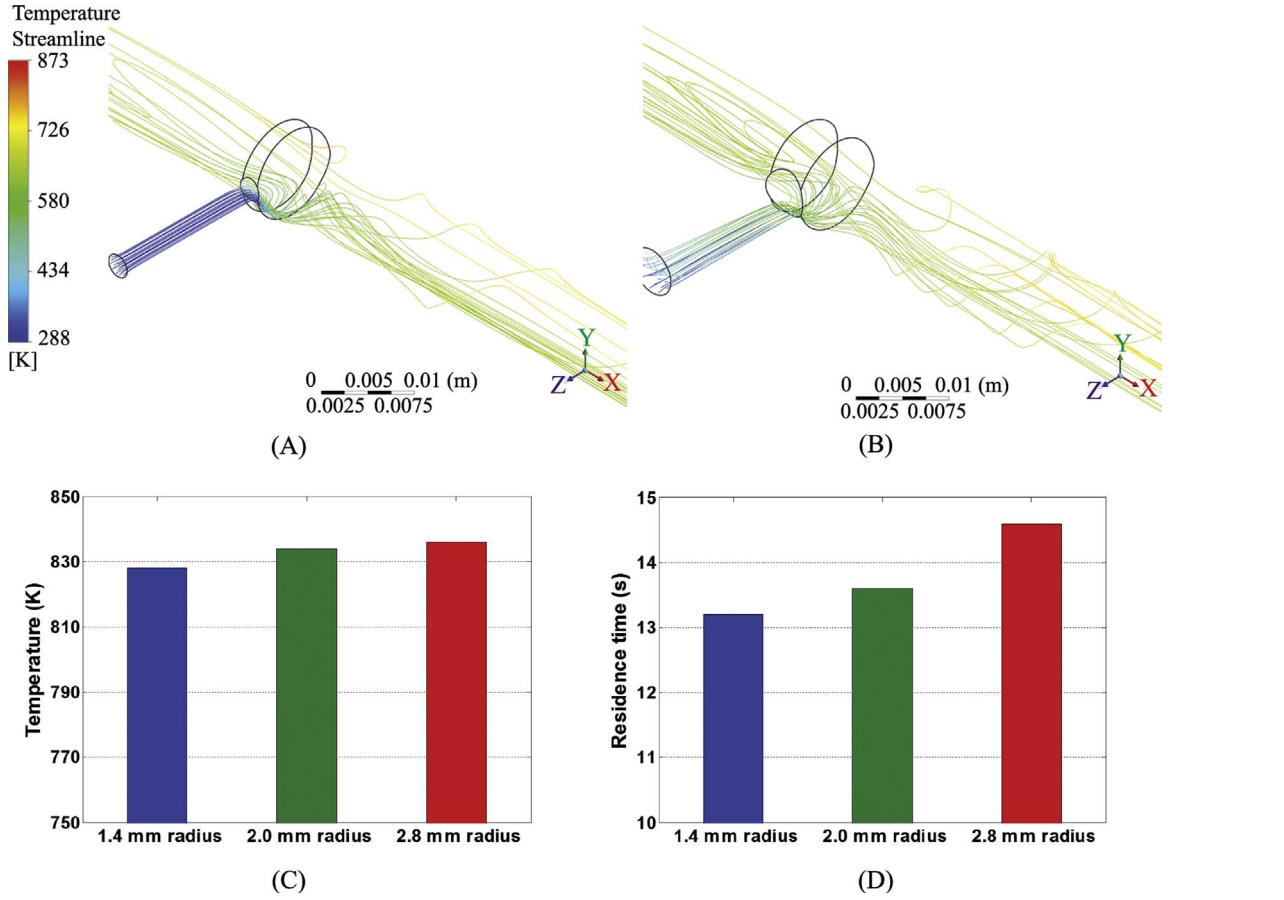

Fig. 14. (A–D) Flow with a reactor wall temperature of 873 K. (A-B) Temperature streamlines for injection tubes with inner diameter of 2.8 mm and 5.6 mm. (C-D) Comparison of outlet temperature and residence time for simulation with different injection tube sizes.

conditions were studied using this model. The model slightly overestimates the outlet temperature in average 6%, which might be due to neglecting the influence of the tube wall thickness. There is also discrepancy in the predicted carbon gasification efficiency in comparison to experimental data on average by 24%. This discrepancy is reduced to 16% when implementing the expanded Arrhenius formula.

Numerical results show that the process experiences several flow swirls that create non-uniform concentration and temperature distribution. Therefore, implementing the reaction kinetics that is derived from experimental investigation that assumes a plug flow reactor with isothermal condition might be the reason of the discrepancies in the carbon gasification efficiency. Another possible reason might be due to the influence of a phase-mass boundary interaction, which is not considered in the model. In general, it can be concluded that the model provides good estimation of the processes occurring during supercritical water gasification.

In addition to model validation, a sensitivity analysis was performed taking into account the influence of gravity and biomass injection velocity. It was observed that the gravitational force induces swirling motions along the flow in the reactor which significantly affect its mixing and heat transfer. Neglecting the gravitational force is demonstrated to underestimate the outlet temperature by approximately 6% in comparison to the standard case (gravity in y positive direction). The research shows that the best position for the reactor tube reactor is horizontal while the injection tube is placed in either the side or the bottom part of the main tube. This can lead to a flow with the most optimum residence time and sufficient swirling to promote the glycerol mixing and heat transfer. It is also revealed that a flow recirculation might take place inside the injection tube, which results in a gradual partial heating of the injected flow that can subsequently lead to char formation. Therefore, it is suggested to utilize a smaller injection tube or to increase the injection flow rate, as these can forcefully reduce this flow recirculation inside the injection tube.

Acknowledgements

This work is supported by the AgentschapNL (RVO) TKI – Scarlet plus programme. For this, the authors would like to express their gratitude. The authors would also like to convey their thanks to all project partners involved within this framework, especially to Jo Penninger (SPARQLE International b.v.) who passed away before this publication was finished.

References

[1] A. Kruse, Hydrothermal biomass gasification, J. Supercrit. Fluids 47 (2009) 391–399.
[2] D. Mohan, C.U. Pittman, P.H. Steele, Pyrolysis of Wood/Biomass for bio-oil: a critical review, Energy Fuels 20 (2006) 848–889.
[3] Process The potential for biomass in the energy mix, Filtr. Sep. 43 (2006) 28–30.
[4] P.E. Savage, S. Gopalan, T.I. Mizan, C.J. Martino, E.E. Brock, Reactions at supercritical conditions: applications and fundamentals, AIChE J. 41 (1995) 1723–1778.
[5] M.J. Antal, S.G. Allen, D. Schulman, X. Xu, R.J. Divilio, Biomass gasification in supercritical water, Ind. Eng. Chem. Res. 39 (2000) 4040–4053.
[6] Y. Matsumura, T. Minowa, B. Potic, S.R.A. Kersten, W. Prins, W.P.M. van Swaaij, B. van de Beld, D.C. Elliott, G.G. Neuenschwander, A. Kruse, M. Jerry Antal Jr, Biomass gasification in near- and super-critical water: status and prospects, Biomass Bioenergy 29 (2005) 269–292.
[7] A. Kruse, Supercritical Water Gasification, (2008).
[8] O. Yakaboylu, J. Harinck, K. Smit, W. de Jong, Supercritical water gasification of biomass: a literature and technology overview, Energies 8 (2015) 859.
[9] A. Chuntanapum, Y. Matsumura, Char formation mechanism in supercritical water gasification process: a study of model compounds, Ind. Eng. Chem. Res. 49 (2010) 4055–4062.
[10] H. Zöhrer, F. Mayr, F. Vogel, Stability and performance of ruthenium catalysts

based on refractory oxide supports in supercritical water conditions, Energy Fuels 27 (2013) 4739–4747.
[11] X. Cheng, B. Kuang, Y.H. Yang, Numerical analysis of heat transfer in supercritical water cooled flow channels, Nucl. Eng. Des. 237 (2007) 240–252.
[12] D. Palko, H. Anglart, Theoretical and numerical study of heat transfer deterioration in high performance light water reactor, Sci. Technol. Nucl. Install. 2008 (2008) 5.
[13] Q.L. Wen, H.Y. Gu, Numerical simulation of heat transfer deterioration phenomenon in supercritical water through vertical tube, Ann. Nucl. Energy 37 (2010) 1272–1280.
[14] Y. Zhang, C. Zhang, J. Jiang, Numerical simulation of heat transfer of supercritical fluids in circular tubes using different turbulence models, J. Nucl. Sci. Technol. 48 (2011) 366–373.
[15] M. Jaromin, H. Anglart, A numerical study of heat transfer to supercritical water flowing upward in vertical tubes under normal and deteriorated conditions, Nucl. Eng. Des. 264 (2013) 61–70.
[16] D. Huang, Z. Wu, B. Sunden, W. Li, A brief review on convection heat transfer of fluids at supercritical pressures in tubes and the recent progress, Appl. Energy 162 (2016) 494–505.
[17] A. Raghavan, A.F. Ghoniem, Simulation of supercritical water-hydrocarbon mixing in a cylindrical tee at intermediate Reynolds number: formulation, numerical method and laminar mixing, J. Supercrit. Fluids 92 (2014) 31–46.
[18] S. Moussière, C. Joussot-Dubien, P. Guichardon, O. Boutin, H.A. Turc, A. Roubaud, B. Fournel, Modelling of heat transfer and hydrodynamic with two kinetics approaches during supercritical water oxidation process, J. Supercrit. Fluids 43 (2007) 324–332.
[19] A.K. Goodwin, G.L. Rorrer, Modeling of supercritical water gasification of xylose to hydrogen-rich gas in a hastelloy microchannel reactor, Ind. Eng. Chem. Res. 50 (2011) 7172–7182.
[20] T. Yoshida, Y. Matsumura, Reactor Development for supercritical water gasification of 4.9 wt% glucose solution at 673 k by using computational fluid dynamics, Ind. Eng. Chem. Res. 48 (2009) 8381–8386.
[21] X. Su, H. Jin, S. Guo, L. Guo, Numerical study on biomass model compound gasification in a supercritical water fluidized bed reactor, Chem. Eng. Sci. 134 (2015) 737–745.
[22] H. Jin, S. Guo, L. Guo, C. Cao, A mathematical model and numerical investigation for glycerol gasification in supercritical water with a tubular reactor, J. Supercrit. Fluids 107 (2016) 526–533.
[23] I.-G. Lee, M.-S. Kim, S.-K. Ihm, Gasification of glucose in supercritical water, Ind. Eng. Chem. Res. 41 (2002) 1182–1188.
[24] W. Hack, D.A. Masten, S.J. Buelow, Methanol and Ethanol Decomposition in Supercritical Water, (2004).
[25] A.G. Chakinala, D.W.F. Brilman, W.P.M. Van Swaaij, S.R.A. Kersten, Catalytic and non-catalytic supercritical water gasification of microalgae and glycerol, Ind. Eng. Chem. Res. 49 (2010) 1113–1122.
[26] J.G. van Bennekom, R.H. Venderbosch, D. Assink, H.J. Heeres, Reforming of methanol and glycerol in supercritical water, J. Supercrit. Fluids 58 (2011) 99–113.
[27] S. Guo, L. Guo, C. Cao, J. Yin, Y. Lu, X. Zhang, Hydrogen production from glycerol by supercritical water gasification in a continuous flow tubular reactor, Int. J. Hydrog. Energy 37 (2012) 5559–5568.
[28] I. ANSYS, ANSYS Fluent Theory Guide 184 ANSYS, Inc., U.S.A, 2015, pp. 56–63.
[29] J. Warnatz, R.W. Dibble, U. Maas, Combustion: Physical and Chemical Fundamentals, Modeling and Siulation, Experiments, Pollutant Formation, 4th ed., Springer, 2006.
[30] G. Dutta, R. Maitri, C. Zhang, J. Jiang, Numerical models to predict steady and unsteady thermal-hydraulic behaviour of supercritical water flow in circular tubes, Nucl. Eng. Des. 289 (2015) 155–165.
[31] K. Wang, X. Xu, Y. Wu, C. Liu, C. Dang, Numerical investigation on heat transfer of supercritical CO2 in heated helically coiled tubes, J. Supercrit. Fluids 99 (2015) 112–120.
[32] P. Basu, V. Mettanant, Biomass gasification in supercritical water – a review, Int. J. Chem. React. Eng. 7 (2009).
[33] M.H. Waldner, Catalytic Hydrothermal Gasification of Biomass for the Production of Synthetic Natural Gas, Eidgenössische Technische Hochschule/Paul Scherrer Institute, Zürich, Switzerland, 2007.
[34] J.A.M. Withag, J.L.H.P. Sallevelt, D.W.F. Brilman, E.A. Bramer, G. Brem, Heat transfer characteristics of supercritical water in a tube: application for 2D and an experimental validation, J. Supercrit. Fluids 70 (2012) 156–170.
[35] W. Wagner, H.-J. Kretzchmar, International Steam Tables: Properties of Water and Steam Based on the Industrial Formulation IAPWS-IF97, 2nd ed., Springer, 2007.
[36] C.M. Huelsman, P.E. Savage, Reaction pathways and kinetic modeling for phenol gasification in supercritical water, J. Supercrit. Fluids 81 (2013) 200–209.
[37] T.H. Chung, M. Ajlan, L.L. Lee, K.E. Starling, Generalized multiparameter correlation for nonpolar and polar fluid transport properties, Ind. Eng. Chem. Res. 27 (1988) 671–679.
[38] R.H. Aungier, A. Fast, Accurate real gas equation of state for fluid dynamic analysis applications, J. Fluids Eng. 117 (1995) 277–281.
[39] I. ANSYS, ANSYS Fluent User's Guide, (2015), pp. 498–499 (U.S.A).
[40] NASA, Chemical Equilibrium Thermo Build, https://www.grc.nasa.gov/WWW/CEAWeb/ceaThermoBuild.htm.
[41] R.F. Susanti, L.W. Dianningrum, T. Yum, Y. Kim, B.G. Lee, J. Kim, High-yield hydrogen production from glucose by supercritical water gasification without added catalyst, Int. J. Hydrog. Energy 37 (2012) 11677–11690.
[42] C.-H. He, Prediction of binary diffusion coefficients of solutes in supercritical solvents, AIChE J. 43 (1997) 2944–2947.
[43] A.L. Magalhães, S.P. Cardoso, B.R. Figueiredo, F.A. Da Silva, C.M. Silva, Revisiting the Liu-Silva-Macedo model for tracer diffusion coefficients of supercritical, liquid, and gaseous systems, Ind. Eng. Chem. Res. 49 (2010) 7697–7700.
[44] X. Lei, H. Li, S. Yu, T. Chen, Numerical investigation on the mixed convection and heat transfer of supercritical water in horizontal tubes in the large specific heat region, Comput. Fluids 64 (2012) 127–140.
[45] Z. Shang, S. Chen, Numerical investigation of diameter effect on heat transfer of supercritical water flows in horizontal round tubes, Appl. Therm. Eng. 31 (2011) 573–581.
[46] M.C. Soteriou, A.F. Ghoniem, Effects of the free-stream density ratio on free and forced spatially developing shear layers, Phys. Fluids 7 (1995) 2036–2051.
[47] A. Raghavan, A.F. Ghoniem, Simulation of supercritical water-hydrocarbon mixing in a cylindrical tee at intermediate Reynolds number: impact of temperature difference between streams, J. Supercrit. Fluids 95 (2014) 325–338.